Journal of The Electrochemical Society, **157** (3) H318-H322 (2010)
0013-4651/2010/157(3)/H318/5/$28.00 © The Electrochemical Society

Fast-Switching Electrochromic Li^+-Doped NiO Films by Ultrasonic Spray Deposition

Robert C. Tenent,[z] Dane T. Gillaspie,[*] Alex Miedaner, Philip A. Parilla, Calvin J. Curtis, and Anne C. Dillon[*]

National Renewable Energy Laboratory, Golden, Colorado 80401, USA

A low cost, high throughput deposition method for films of nickel oxide (NiO) and lithium-doped nickel oxide with improved electrochromic performance is demonstrated. This method is based on ultrasonic spray deposition of aqueous-based precursor solutions in air at atmospheric pressure, which represents a significant cost savings compared to vacuum deposition methods. The resultant materials are characterized by X-ray diffraction, Raman spectroscopy, electron microscopy, and electrochemical measurements. Electrochromic performance is demonstrated with in situ optical transmission measurements during electrochemical characterization. Nickel oxide materials color anodically and are thereby ideally suited to be used as counter electrode for the well-known tungsten oxide (WO_3) system in "smart" window applications. The coloration of nickel oxide materials is known to be slow when compared to WO_3 and thereby limits the overall response time of a NiO/WO_3 tandem device. The analysis of potential step response data shows that our lithium-doped nickel oxide material achieves 90% of its total coloration change in 29 s, which is comparable to reported measurements for WO_3. These results significantly mitigate a potential bottleneck to the adoption of metal oxide electrochromic windows not only by demonstrating similar performance between NiO and WO_3, but by achieving this result via low cost, highly scalable processing methods.
 [DOI: 10.1149/1.3279992]

Manuscript submitted August 31, 2009; revised manuscript received November 25, 2009. Published January 19, 2010.

Internal environmental control of buildings is responsible for a significant portion of overall electricity use in the U.S.[1] Energy-efficient "smart" windows that can change transmission characteristics in response to external stimuli are poised to make a tremendous impact by reducing the energy needed to maintain comfortable building environments as well as providing controllable daylighting for building occupants. One method to accomplish this is to employ electrochromic (EC) metal oxide films, where the optical transmission may be modulated to pass or block incident sunlight by applying a small voltage. However, widespread implementation of smart windows depends critically on developing cost-effective techniques that can also be integrated into large-scale manufacturing. EC metal oxide films are typically deposited by vacuum deposition methods, primarily sputtering,[2-7] although several alternate processes have been demonstrated.[6,8-16] It is believed that a simple spray-coating deposition method, which can be performed using aqueous-based liquid precursor materials in air, is a candidate for an even more cost-effective and widely implementable production method.

The operation of conventional inorganic EC devices depends on a reversible electrochemical double injection of positive ions (H^+, Li^+, Na^+, and K^+) and electrons into the host lattice of multivalent transition-metal oxide materials.[17,18] Tungsten oxide (WO_3) is the most established EC material for the active (coloring) electrode.[19-23] It shows cathodic coloration with electron injection and charge-balancing ion insertion. Alternately, some EC materials color anodically by the removal of electrons and positive ions.[24] The most frequently studied materials with anodic coloration are nickel oxide and iridium oxide. By combining an electrode that exhibits cathodic coloration with a counter electrode that has anodic coloration, it is possible to fabricate a more efficient and visually appealing EC device. One such EC system that has seen intense interest of late uses WO_3 as the active electrode and NiO as a counter electrode.[25-27]

Here, we present spray deposition methods for nickel oxide and lithium-doped nickel oxide films for use as a complementary and anodically coloring counter electrode for the well-known WO_3 system. Our interest in the Li-doped NiO material is based on reported longer device lifetimes for Li-ion-based EC devices that employ nonaqueous electrolytes.[7] Several processes have been demonstrated for spray-coating NiO films.[28-42] Significantly fewer papers have discussed spray deposition methods for lithium-doped NiO films,[43-45] and none to date have studied the performance of such films in EC applications. Furthermore, the literature on spray coating of EC NiO films has predominantly focused on the KOH-based aqueous electrolyte system.

Our deposition process is based on the ultrasonic spraying method, which holds several key advantages over more widely employed pressure-driven spraying methods. Among these are lower materials usage and improved uniformity due to a narrower size distribution of droplets in the atomized material.[46] In brief, a liquid precursor solution is pumped to an ultrasonically excited tip surface. Standing waves form in the liquid layer on the nozzle surface. These waves become unstable at their peaks and collapse, leading to the generation of fine droplets of the precursor solution. The atomized material is carried by a controlled nitrogen flow to a heated substrate where it undergoes thermal decomposition to yield the desired film. We have used this technique to spray deposit both NiO and lithium-doped NiO films. Furthermore, although NiO has previously been shown to act successfully as a counter electrode for the WO_3 system, ion movement into and out of the NiO structure is reported to be slower than for WO_3, thereby limiting the switching speed and overall device performance.[47] Here, we have also demonstrated improved kinetics for our lithium-doped NiO film, indicating that these films are more promising as a counter electrode when employing WO_3 as the active electrode.

Experimental

Chemicals.— Nickel nitrate and lithium nitrate salts were obtained from Aldrich and used as received. All solutions for spray deposition were made with deionized water. Premade electrolyte solutions for electrochemical testing were obtained from Ferro Corporation (Zachary, LA).

Spray apparatus.— The ultrasonic spray system was from Sono-Tek Corporation and consisted of a model 8700-120 spray head that operated at a frequency of 120 kHz. A Sono-Tek Broadband Ultrasonic Generator was used to apply ultrasonic excitation to the spray nozzle, which had a 0.230 in. diameter conical tip and a 0.015 in. diameter orifice that was fitted with the impact system for gas-driven spray delivery. A controlled gas flow was supplied by a model FMA 1818 mass flowmeter from Omega Engineering, Inc., which delivered the atomized material to the surface. The precursor solution was pumped to the spray nozzle through a Fluid Metering Inc. VMP TRI Pulseless "Smoothflow" pump equipped with three model Q1-CSC-W-LF pump heads.

* Electrochemical Society Active Member.
[z] E-mail: Robert.Tenent@nrel.gov

Substrate materials and preparation.— All films for electro-optical characterization were deposited on fluorine-doped tin oxide (FTO) films. Films for X-ray diffraction (XRD) and Raman analysis were deposited on glass microscope slides. Before deposition, all substrates were cleaned with an isopropanol-soaked clean-room wipe, blown dry with nitrogen, and then placed in an oxygen plasma (800 mTorr, 155 W) for 5 min.

XRD.— Data were collected using a Bruker AXS D8 Discover with a HiStar area detector. For the XRD measurements, the sample was illuminated with X-rays from a copper target (40 kV, 35 mA) using a Göebel mirror and a 1 mm circular collimator. The recorded XRD signals contained both Kα1 and Kα2 components, but no Kβ component as it was filtered out by the Göebel mirror. The two-dimensional area detector data were integrated in chi using GADDS software to produce a more conventional XRD intensity vs 2θ data plot. Background data for FTO substrates were collected and subtracted from sample films.

Raman spectroscopy.— Spectra were collected using 2.54 eV (488 nm) laser excitation. The backscattered light was analyzed with a Jobin Yvon 270M spectrometer equipped with a liquid-nitrogen-cooled Spectrum One charge-coupled device and a holographic notch filter. A Nikon 55 mm camera lens was employed both to focus the beam on the sample to an ~0.25 mm^2 spot and to collect the Raman scattered light. Averaging three 60 s scans was sufficient to obtain high intensity, well-resolved Raman spectra.

Electrochemical analysis.— Cyclic voltammetry and potential cycling measurements were made using a BioLogic VMP3 multichannel potentiostat. Samples were examined in a two-electrode testing mode vs a Li metal counter electrode in 1 M Li perchlorate dissolved in propylene carbonate. All electrochemical testing was performed inside a controlled atmosphere glove box from Vacuum Atmospheres Corporation. All voltammetric scans were collected at a 20 mV/s scan rate and all electrodes tested were 1 cm^2 in geometric surface area.

Transmission measurements.— In situ optical transmission measurements employed a diode laser operating at 670 nm as the source and a Thor Labs, Inc. DET100A large-area silicon detector. Clean, uncoated, FTO substrates were used to set the 100% transmission level of the detector before obtaining sample measurements.

Results and Discussion

Deposition chemistry.— Figure 1 shows thermogravimetric analysis (TGA) data for both nickel and lithium nitrate salts collected under a "pseudo" air mixture (80% nitrogen, 20% oxygen). Decomposition of $NiNO_3 \cdot 6H_2O$ appears to come to completion near 325°C. The mass loss up to 250°C is consistent with dehydration of the starting material, whereas the mass loss finishing at 325°C is consistent with loss of nitrate ion. The final percentage of the original mass is below what would be expected for the conversion of the nickel salt to NiO under these conditions, which may indicate substoichiometry in the final product. Although TGA data are useful for predicting optimal deposition temperatures for the spray process, they do not necessarily indicate the exact products that will form. Figure 1 also shows the TGA data for lithium nitrate that does not show significant mass loss until ~600°C, although differential thermal analysis confirmed a melting point of ~260°C. Attempts to produce films at ~600°C led to the deformation of the underlying FTO-coated glass substrate. It is unclear if this was due to glass deformation or damage to the FTO layer itself. Gordon reported instability for FTO in this temperature range.[48] Based on these results, the spray depositions reported here were performed at 330°C, which was a sufficiently high temperature to decompose the nickel nitrate as well as to melt the additional lithium nitrate. This is potentially an important point as several papers have reported improved performance for ceramic materials sintered in the presence of a liquid phase.[49-51]

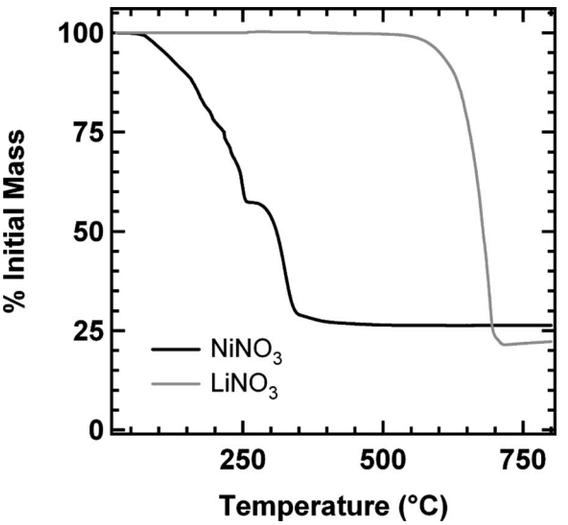

Figure 1. Thermogravimetric data for $NiNO_3$ and $LiNO_3$ under a pseudoair mixture.

Figure 2 shows XRD data and Raman spectra for films sprayed from nickel nitrate solutions with and without 5 wt % $LiNO_3$ added. The lithium nitrate loading level was fixed based on separate experiments that demonstrated no significant improvement in film performance for loadings higher than 5% (data not shown). This agrees with the recent paper of Joseph et al., who spray-coated lithium-doped NiO films for use in dye-sensitized solar cells.[45] Figure 2a shows XRD data for films sprayed with and without lithium doping. The film sprayed from $NiNO_3$ clearly shows peaks indicating the formation of nickel oxide (JCPDS file no. 47-1049), with the (200) peak being dominant as expected for a randomly oriented film. XRD data for the Li-doped material show identical peaks for NiO formation as well as other peaks that can be attributed to unreacted lithium nitrate (JCPDS file no. 08-0466) (denoted with an asterisk). No peaks are observed that can be correlated to previously reported LiNiO crystal structures. Figure 2b shows Raman spectroscopy data for the same samples. The spectra of both the NiO and lithium-doped NiO films exhibit a peak at ~500 cm^{-1}, which is consistent with previously reported excitation of the NiO stretching vibrations.[52-54] No apparent shift is observed upon adding lithium ions to the film. The improved EC performance of the lithium-doped materials (discussed below) combined with the XRD and Raman data raises the suggestion that both amorphous LiNiO and NiO crystallites may be present in our material. Lithium–cobalt spinel structures have been prepared under similar conditions by reaction of CoOOH and $LiNO_3$.[55]

EC performance.— Figure 3 shows cyclic voltammetry coupled with optical transmission data collected at 670 nm for films sprayed from nickel nitrate with and without lithium nitrate added. Although both films were sprayed to approximately the same thickness, the Li-doped material clearly shows both higher charge insertion upon cycling and, subsequently, a larger transmission change. The voltammetry for the Li-doped material also shows more defined peaks for lithium intercalation and deintercalation than for the undoped NiO material. The better-defined peaks and the more rapid increase in current as a function of potential indicate a larger and faster ion intercalation into the doped material as compared to NiO only.

Figure 4 shows transmission data for the same samples as shown in Fig. 3 under potential step cycling from 2.25 to 4.25 V vs Li/Li^+. The Li-doped material shows a significantly higher transmission modulation (~83 to ~33%) than the accompanying NiO material (36–19%). These values are slightly different from those observed in

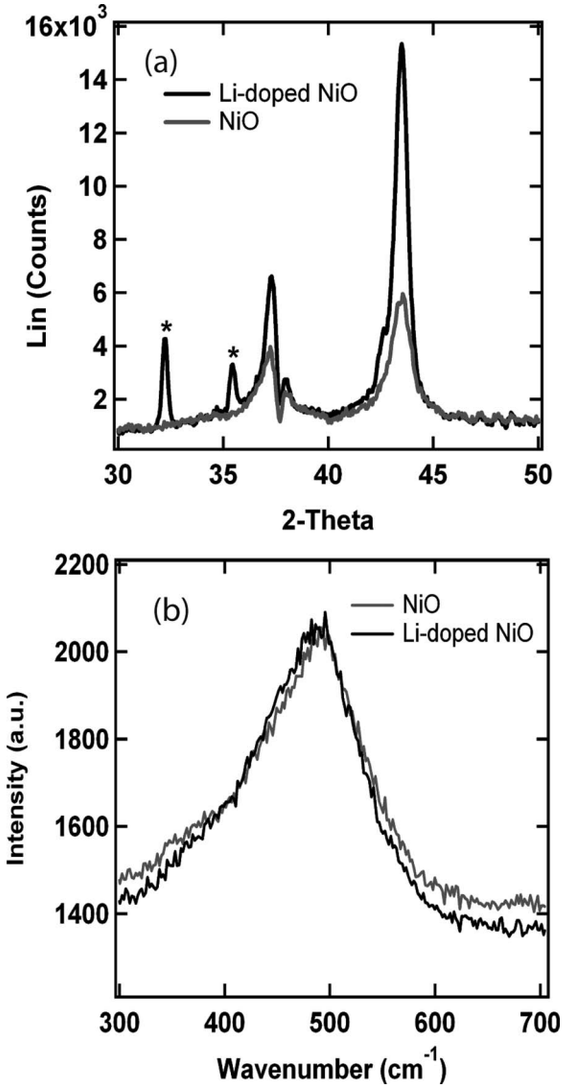

Figure 2. (a) XRD and (b) Raman spectroscopy data for as-deposited films sprayed from $NiNO_3$ with and without $LiNO_3$ added.

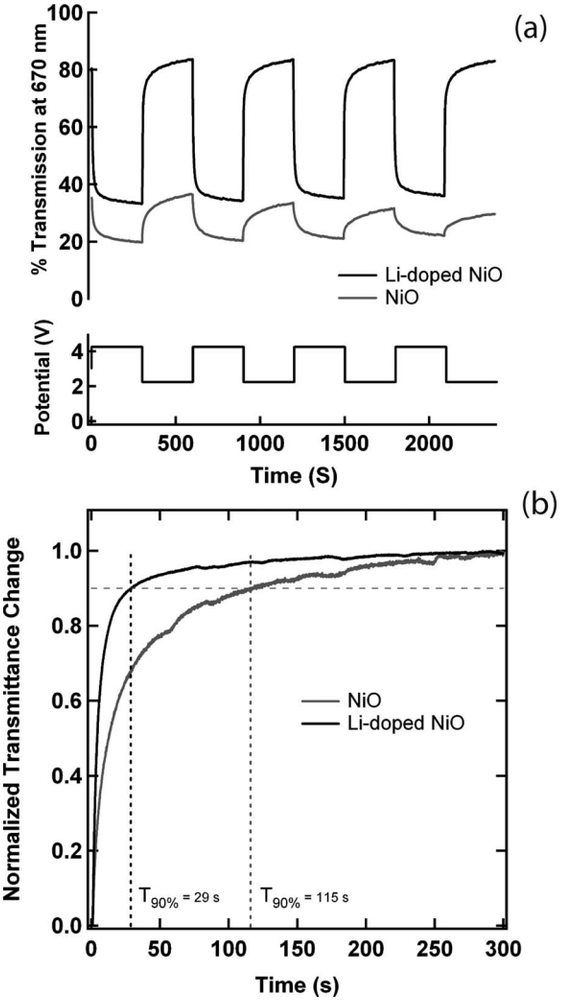

Figure 4. (a) Optical transmission response from the same samples discussed in Fig. 3 under potential step cycling between 4.25 and 2.25 V vs Li/Li^+. (b) Normalized transmission as a function of time extracted from one cycle of the data shown in (a). Transmission was normalized to the final transmission obtained after 5 min at potential.

Fig. 3 due to longer times (5 min) spent at potential extremes than were employed for the voltammetric scans. Coloration efficiency (CE) is one of the most important metrics for selecting an EC material and is defined as the change in optical density (OD) per unit inserted charge (Q), i.e., $CE = \Delta(OD)/\Delta Q$. Analysis of the data for the Li-doped material yields a CE of 33 cm^2/C, which is comparable to that measured for sputtered films.[2] The transmission modulation of the NiO film is already starting to degrade in this limited number of potential cycles. In contrast, the Li-doped material appears to show improved cycling stability compared to the NiO material. However, longer-term cycling (50 cycles) demonstrated a significant, albeit slower, decrease in transmission modulation for the Li-doped films, which is well known for NiO materials[56] and remains a weakness of the present system (data not shown).

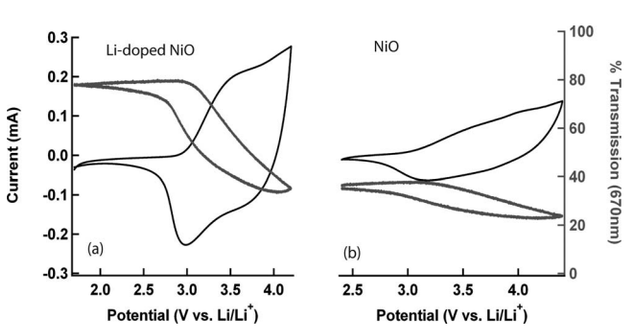

Figure 3. Cyclic voltammetry for films spray-coated from $NiNO_3$ (a) with and (b) without $LiNO_3$ present. The vertical axes are identical for both plots. The vertical axes in the center of the figure have been deleted to allow a less cluttered view of the data.

In addition to the larger transmission change, the Li-doped material has a faster coloration change than the NiO material. This is clearly demonstrated in Fig. 4b, which shows normalized transmission data for samples sprayed from nickel nitrate with and without lithium nitrate. These data are for the coloration of the NiO-based devices, and the switching speed is reported as the time to achieve 90% of the total coloration change. NiO shows a typical slow coloration process, reaching 90% of its change in 115 s. However, the Li-doped film achieves the same coloration change in about 29 s in addition to having a significantly larger change in transmission. Similar measurements for the bleaching step show that the Li-doped

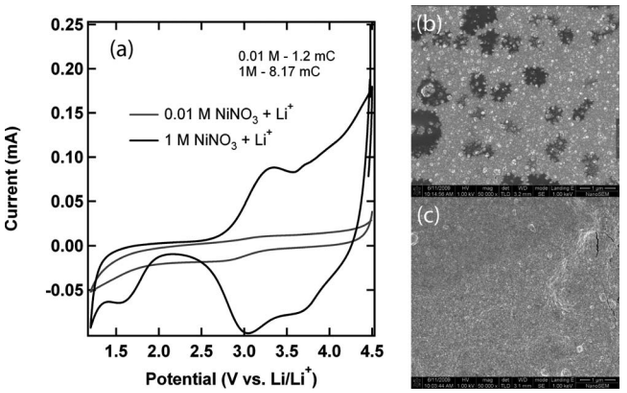

Figure 5. (a) Cyclic voltammetry for lithium-doped nickel oxide films sprayed from differing precursor concentrations and SEM micrographs of the same films sprayed from (b) 10 mM and (c) 1 M $NiNO_3$. Both samples had 5 wt % $LiNO_3$ added.

NiO film bleaches in 57 s. These switching speeds are comparable to those reported for WO_3 films by Deepa et al.[57] for sol–gel-processed materials and Subrahmanyam et al.[58] for oxygen-sputtered materials. This demonstrates that our Li-doped films are extremely promising for a counter electrode in an inexpensively processed EC device employing a WO_3 film as the active electrode.

Effect of surface morphology.— One inherent advantage of a liquid precursor spray-based process is the ability to tune film morphology by making simple changes in material formulation. For example, a lower concentration of precursor material per drop of atomized ink should lead to smaller crystallite sizes upon drop drying. Attempts were made to determine the effect of morphology on EC film performance by varying the precursor salt concentrations. We hypothesized that a smaller crystallite size would lead to more facile Li-ion intercalation upon cycling. The concentration of the nickel nitrate precursor with 5% (w/w) lithium nitrate was varied from 10 mM to 1 M. Films were spray-coated to identical thickness by varying the number of coats based on the solution concentration. For example, while only a single coating was deposited with the 1 M concentration, the sample from the 10 mM precursor salt required 100 coatings. Figure 5a shows the cyclic voltammetry data collected for these films. The film deposited from the 1 M concentration clearly shows a higher charge injection than the film deposited from the 10 mM solution. The scanning electron microscope (SEM) images on the right likely explain the voltammetric results. The top image (Fig. 5b) is of the film deposited from the 10 mM solution, and the bottom image (Fig. 5c) is of the film deposited from the 1 M solution. The expected trend in crystallite size is the opposite of what was originally anticipated; furthermore, phase separation is clearly evident for the 10 mM film. The 1 M film appears significantly more uniform and does not show phase separation. This observation can be rationalized by taking into account the total time for each deposition process. The attempt to maintain the same final film thickness while changing the precursor concentration led to excessively long deposition times for the 10 mM sample (~60 min). The longer exposure to high temperature (330°C) resulted in the annealing of the film, causing phase separation and particle agglomeration. The 1 M film was deposited in under 60 s and clearly yields superior performance.

Conclusions

We have demonstrated an inexpensive, mass-production-friendly, Li-doped NiO EC material that yields similar performance to vacuum-deposited materials. The exact composition and structure of the material are unclear, but the material is likely an amorphous LiNiO matrix that contains NiO crystallites, as indicated by XRD and Raman spectroscopy. Furthermore, the switching speed for coloration and bleaching of the film is comparable to that for WO_3, thereby demonstrating excellent potential for use as a counter electrode in an EC device. Attempts to modulate film morphology by changing precursor concentration indicated that higher concentrations deposited quickly yield better EC performance. When lower concentrations are employed, excessively long deposition times are required that lead to particle agglomeration and poor performance.

Acknowledgments

The authors acknowledge Dr. Maikel van Hest for assistance with the ultrasonic spray deposition and useful discussions on potential precursor materials. This work was funded by the U.S. Department of Energy (DOE) under subcontract no. DE-AC36-08GO28308 through the DOE Office of Energy Efficiency and Renewable Energy, Office of Building Technologies Program.

National Renewable Energy Laboratory assisted in meeting the publication costs of this article.

References

1. Energy Information Administration, *Annual Energy Review*, p. 446, Department of Energy, Washington, DC (2009).
2. F. Michalak, K. von Rottkay, T. Richardson, J. Slack, and M. Rubin, *Electrochim. Acta*, **44**, 3085 (1999).
3. S. Passerini, B. Scrosati, and A. Gorenstein, *J. Electrochem. Soc.*, **137**, 3297 (1990).
4. B. Passerini and S. Scrosati, *Solid State Ionics*, **53–56**, 520 (1992).
5. B. Passerini and S. Scrosati, *J. Electrochem. Soc.*, **141**, 889 (1994).
6. M. Rubin, S. J. Wen, T. Richardson, J. Kerr, K. von Rottkay, and J. Slack, *Sol. Energy Mater. Sol. Cells*, **54**, 59 (1998).
7. T. Kubo, Y. Nishikitani, Y. Sawai, H. Iwanaga, Y. Sato, and Y. Shigesato, *J. Electrochem. Soc.*, **156**, H629 (2009).
8. I. Bouessay, A. Rougier, B. Beaudoin, and J. B. Leriche, *Appl. Surf. Sci.*, **186**, 490 (2002).
9. F. I. Ezema, A. B. C. Ekwealor, and R. U. Osuji, *J. Optoelectron. Adv. Mater.*, **9**, 1898 (2007).
10. S. Y. Han, D. H. Lee, Y. J. Chang, S. O. Ryu, T. J. Lee, and C. H. Chang, *J. Electrochem. Soc.*, **153**, C382 (2006).
11. U. M. Patil, R. R. Salunkhe, K. V. Gurav, and C. D. Lokhande, *Appl. Surf. Sci.*, **255**, 2603 (2008).
12. M. Ristova, J. Velevska, and M. Ristov, *Sol. Energy Mater. Sol. Cells*, **71**, 219 (2002).
13. M. A. Vidales-Hurtado and A. Mendoza-Galvan, *Mater. Chem. Phys.*, **107**, 33 (2008).
14. M. A. Vidales-Hurtado and A. Mendoza-Galvan, *Solid State Ionics*, **179**, 2065 (2008).
15. X. H. Xia, J. P. Tu, J. Zhang, X. L. Wang, W. K. Zhang, and H. Huang, *Sol. Energy Mater. Sol. Cells*, **92**, 628 (2008).
16. X. H. Xia, J. P. Tu, J. Zhang, X. L. Wang, W. K. Zhang, and H. Huang, *Electrochim. Acta*, **53**, 5721 (2008).
17. S. K. Deb, *Philos. Mag.*, **27**, 801 (1973).
18. S.-H. Lee, H. M. Cheong, J.-G. Zhang, A. Mascarenhas, D. K. Benson, and S. K. Deb, *Appl. Phys. Lett.*, **74**, 242 (1999).
19. S. H. Lee, H. M. Cheong, C. E. Tracy, A. Mascarenhas, A. W. Czanderna, and S. K. Deb, *Appl. Phys. Lett.*, **75**, 1541 (1999).
20. C. Bechinger, M. S. Burdis, and J. G. Zhang, *Solid State Commun.*, **101**, 753 (1997).
21. S. S. Sun and P. H. Hollway, *J. Vac. Sci. Technol. A*, **2**, 336 (1984).
22. S.-H. Lee, R. Deshpande, P. A. Parilla, K. M. Jones, B. To, A. H. Mahan, and A. C. Dillon, *Adv. Mater.*, **18**, 763 (2006).
23. N. A. Chernova, M. Roppolo, A. C. Dillon, and M. S. Whittingham, *J. Mater. Chem.*, **19**, 2526 (2009).
24. C. G. Granqvist, *Handbook of Inorganic Electrochromic Materials*, Elsevier, New York (1995).
25. A. Azens, G. Vaivars, M. Veszelei, L. Kullman, and C. G. Granqvist, *J. Appl. Phys.*, **89**, 7885 (2001).
26. C. G. Granqvist, *Sol. Energy Mater. Sol. Cells*, **92**, 203 (2008).
27. R. Lechner and L. K. Thomas, *Sol. Energy Mater. Sol. Cells*, **54**, 139 (1998).
28. J. Arakaki, R. Reyes, M. Horn, and W. Estrada, *Sol. Energy Mater. Sol. Cells*, **37**, 33 (1995).
29. Y. Xie, W. Wang, Y. Qian, L. Yang, and Z. Chen, *J. Cryst. Growth*, **167**, 656 (1996).
30. M. Gómez, A. Medina, and W. Estrada, *Sol. Energy Mater. Sol. Cells*, **64**, 297 (2000).
31. L. D. Kadam and P. S. Patil, *Sol. Energy Mater. Sol. Cells*, **69**, 361 (2001).
32. S. A. Mahmoud, A. A. Akl, H. Kamal, and K. Abdel-Hady, *Physica B*, **311**, 366 (2002).
33. P. S. Patil and L. D. Kadam, *Appl. Surf. Sci.*, **199**, 211 (2002).
34. S.-Y. Wang, W. Wang, W.-Z. Wang, and Y.-W. Du, *Mater. Sci. Eng., B*, **90**, 133 (2002).
35. H. Kamal, E. K. Elmaghraby, S. A. Ali, and K. Abdel-Hady, *Thin Solid Films*,

483, 330 (2005).
36. J. D. Desai, S.-K. Min, K.-D. Jung, and O.-S. Joo, *Appl. Surf. Sci.*, **253**, 1781 (2006).
37. H.-S. Kim, C. S. Kim, and S.-G. Kim, *J. Non-Cryst. Solids*, **352**, 2204 (2006).
38. B. A. Reguig, M. Regragui, M. Morsli, A. Khelil, M. Addou, and J. C. Bernède, *Sol. Energy Mater. Sol. Cells*, **90**, 1381 (2006).
39. B. A. Reguig, A. Khelil, L. Cattin, M. Morsli, and J. C. Bernède, *Appl. Surf. Sci.*, **253**, 4330 (2007).
40. L. Cattin, B. A. Reguig, A. Khelil, M. Morsli, K. Benchouk, and J. C. Bernède, *Appl. Surf. Sci.*, **254**, 5814 (2008).
41. S.-H. Lin, F.-R. Chen, and J.-J. Kai, *Appl. Surf. Sci.*, **254**, 2017 (2008).
42. U. P. Muecke, N. Luechinger, L. Schlagenhauf, and L. J. Gauckler, *Thin Solid Films*, **517**, 1522 (2009).
43. P. Puspharajah, S. Radhakrishna, and A. Arof, *J. Mater. Sci.*, **32**, 3001 (1997).
44. N. Kyung-Wan and K. Kwang-Bum, *Electrochemistry (Tokyo, Jpn.)*, **69**, 467 (2001).
45. D. P. Joseph, M. Saravanan, B. Muthuraaman, P. Renugambal, S. Sambasivam, S. P. Raja, P. Maruthamuthu, and C. Venkateswaran, *Nanotechnology*, **19**, 485707 (2008).
46. H. L. Berger, *Ultrasonic Liquid Atomization: Theory and Application*, p. 177, Partridge Hill, Hyde Park, NJ (2006).
47. S. H. Lee and S. K. Joo, *Sol. Energy Mater. Sol. Cells*, **39**, 155 (1995).
48. R. G. Gordon, *Mater. Res. Bull.*, **25**, 52 (2000).
49. V. Esposito, M. Zunic, and E. Traversa, *Solid State Ionics*, **180**, 1069 (2009).
50. J. D. Nicholas and L. C. De Jonghe, *Solid State Ionics*, **178**, 1187 (2007).
51. D. W. Yuan, S. F. Wang, W. Huebner, and G. Simkovich, *J. Mater. Res.*, **8**, 1675 (1993).
52. S. I. Cordoba-Torresi, C. Gabrielli, A. H.-L. Goff, and R. Torresi, *J. Electrochem. Soc.*, **138**, 1548 (1991).
53. R. E. Dietz, G. I. Parisot, and A. E. Meixner, *Phys. Rev. B*, **4**, 2302 (1971).
54. S.-H. Lee, H. M. Cheong, N.-G. Park, C. E. Tracy, A. Mascarenhas, D. K. Benson, and S. K. Deb, *Solid State Ionics*, **140**, 135 (2001).
55. E. Zhecheva and R. Stoyanova, *Mater. Res. Bull.*, **26**, 1315 (1991).
56. I. Bouessay, A. Rougier, P. Poizot, J. Moscovici, A. Michalowicz, and J. M. Tarascon, *Electrochim. Acta*, **50**, 3737 (2005).
57. M. Deepa, T. K. Saxena, D. P. Singh, K. N. Sood, and S. A. Agnihotry, *Electrochim. Acta*, **51**, 1974 (2006).
58. A. Subrahmanyam, A. Karuppasamy, and C. S. Kumar, *Electrochem. Solid-State Lett.*, **9**, H111 (2006).